

# The stratorotational instability of Taylor-Couette flows of moderate Reynolds numbers

G. Rüdiger<sup>1</sup>, T. Seelig<sup>2</sup>, M. Schultz<sup>1</sup>, M. Gellert<sup>1</sup>, U. Harlander<sup>2</sup>,  
Chr. Egbers<sup>2</sup>

<sup>1</sup>Leibniz-Institut für Astrophysik Potsdam, An der Sternwarte 16, D-14467 Potsdam, Germany

<sup>2</sup>Aerodynamik und Strömungslehre, BTU Cottbus – Senftenberg, Siemens-Halske-Ring 14,  
D-03046 Cottbus, Germany

(Received 11 October 2016)

The instability against nonaxisymmetric perturbations of a Taylor-Couette flow with an axial density stratification is considered. The potential flow (driven by cylinders rotating according to the Rayleigh limit) becomes unstable if the Froude number  $Fr$  (= rotation frequency/buoyancy frequency) fulfills  $Fr_{\min} < Fr < Fr_{\max}$  with  $Fr_{\min} \simeq 0.3$  and  $Fr_{\max} \simeq 5.5$  (for a radius ratio of the cylinder radii  $\eta = 0.52$ ). If the rotation law becomes flatter the molecular viscosity stabilizes the flow leaving isolated islands of instability in the rotation/stratification parameter map at moderate Reynolds numbers. For given stratification there is always a lower and upper rotation rate limiting the domain of instability. The values of the lower critical Reynolds number slightly increase with the shear parameter  $\mu = \Omega_{\text{out}}/\Omega_{\text{in}}$  in almost perfect accordance with empirical results obtained with the Cottbus SRI experiment. The upper Reynolds number above which the SRI decays, has its maximum value for the potential flow and decreases strongly for the flatter rotation profiles. Along and between the lines of neutral stability the wave numbers of the instability patterns for all rotation laws beyond the Rayleigh limit and for all Fourier modes  $m$  are mainly determined by  $Fr$ . The cells are thus highly prolate for  $Fr > 1$  so that measurements for too high Reynolds numbers are excluded for axially bounded containers. The instability pattern migrates azimuthally with  $\dot{\phi}/\Omega_{\text{out}} \gtrsim 1$  so that the SRI pattern always drifts (slightly) faster than the outer cylinder rotates. The measurements confirm this prediction with high accuracy.

## 1. Introduction

The magneto-rotational instability (MRI) is now commonly invoked in order to understand the origin of the turbulence in accretion discs. This is because there exist no purely hydrodynamic local instabilities in accretion discs in the sense that a periodic shearing box approach is applied. Already when vertical shear is included, however, there is a linear instability, but its growth rate is small compared with that of the MRI (Urpin & Brandenburg 1998; Arlt & Urpin 2004). Purely hydrodynamic instabilities are of interest for proto-stellar discs where the electric conductivity is usually so low that magnetic effects are unimportant, and hence the MRI may here be irrelevant. Another possibility for a hydrodynamic instability is the nonlinear shear instability (Chagelishvili et al. 2003; Tevade et al. 2008). However, a conclusive solution of this problem using simulations remains difficult because of the large Reynolds numbers required.

For the classical Taylor-Couette flows the rotation law  $\Omega \propto 1/R^2$  (potential flow,

the ‘Rayleigh limit’) separates the unstable-flow region from the stable-flow. The potential flow is curl-free, i.e.  $\text{curl} \mathbf{U} = 0$  while for rigid rotation one has  $\text{curl} \mathbf{U} = 2\boldsymbol{\Omega}$ . Clearly, the potential flow is the flow with the weakest stabilizing properties. Withjack & Chen (1974), however, observed nonaxisymmetric disturbances in density-stratified Taylor-Couette flows beyond the Rayleigh limit. With their wide-gap container the resulting experimental instability line, however, is rather steep (see their Fig. 8) and never crosses the line  $\Omega \propto 1/R$ . One can indeed show theoretically that the combination of stable axial density stratification and centrifugally stable differential rotation leads to a flow which is linearly unstable against nonaxisymmetric perturbations (Molemaker et al. 2001; Yavneh et al. 2001; Dubrulle et al. 2005; Shalybkov & Rüdiger 2005; Umurhan 2006). Dubrulle et al. (2005) found that this instability which is now called the stratorotational instability (SRI) does not require the presence of radial boundaries.

Le Dizes & Riedinger (2010) solved the *inviscid* equations by Yavneh et al. (2001) for the potential flow combining a rigid inner boundary with an infinite gap width and showed that the most unstable modes belong to high azimuthal wave numbers. Weak stratification suppresses the instability. Pure Keplerian rotation – which is not an exact solution of the zero-order equations – proves to be stable for disturbances with azimuthal mode number smaller than 14. The same system of inviscid equations is also reported as allowing instability if the angular velocity of the rotation increases outwards (‘superrotation’, Park & Billant 2013).

Shalybkov & Rüdiger (2005) considered Taylor-Couette flows with finite viscosity in the presence of boundaries and gave stability criterion of the instability. For the considered small gap for a fixed small Froude number of 0.5 the flattest unstable rotation law was  $\Omega \propto 1/R$  which has experimentally been confirmed by Le Bars & Le Gal (2006). In a later publication Rüdiger & Shalybkov (2009) demonstrated that for unity Froude number indeed  $\Omega \propto 1/R$  approaches the smoothest unstable rotation law for a wide variation of the gap width.

In a recent paper Ibanez et al. (2016) reported results of new experiments with a small-gap container ( $\eta = 0.877$ ) with variable rotation laws including the potential flow. Below we shall discuss some of their findings in the light of new experimental and theoretical results.

The paper is organized as follows. In Section 2 we briefly describe the experimental setup and in Section 3 we give details about the Taylor-Couette flow model that is linearized and solved numerically. This is done first in Section 4 where we present stability properties for the most prominent example of potential flow for which the rotation ratio of the cylinders equal the square of the radius ratio. Subsequently, in Section 5 we do the same for flat rotation laws and compare stability diagrams and drift rates with the ones obtained from experimental measurements. Moreover, in Section 6 we discuss the axial wave number of the unstable modes and give limits for the Froude number in view of the finite size of the experimental apparatus. In Section 7 we briefly discuss the stability for modes with larger azimuthal wave numbers and we present growth rates in Section 8. Finally, in Section 9 we give conclusions.

## 2. Experimental realization

The SRI experiment of the BTU Cottbus – Senftenberg is used to probe the main findings of the linear theory by experimental data. In opposition to earlier experiments it works with a stable stratification due to a positive axial temperature gradient  $\partial T/\partial z$  by heating the cylindrical gap from *above* (Gellert & Rüdiger 2009). Instead of the density gradient it is here the temperature gradient that defines the buoyancy frequency

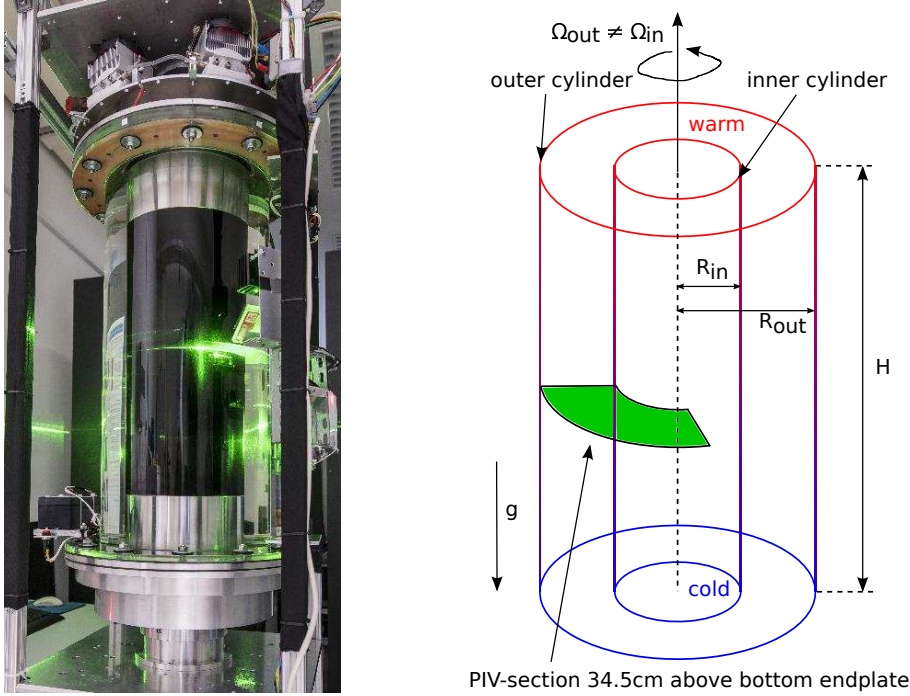


FIGURE 1. Left: Picture of the SRI experiment at the Brandenburgische Technische Universität Cottbus – Senftenberg. Right: Sketch of the experimental cell and position of the PIV-section used to determine the flow state (stable/unstable) and the drift rate.

$N^2 = \alpha g \partial T / \partial z$ , where  $\alpha$  and  $g$  are the coefficient of volume expansion and gravity, respectively. Beyond the Rayleigh limit the unstratified flow is hydrodynamically stable but a destabilization happens already for a temperature difference between top and bottom of a few K. The container has an aspect ratio of  $\Gamma = H / (R_{out} - R_{in}) = 10$  (70 cm height) and a ratio of the cylinder radii of  $\eta = 0.52$  (Fig. 1). Due to the Taylor-Proudman theorem the instability cells become highly elongated so that an aspect ratio of ten only allows not too fast rotation. The temperature difference between top and bottom varies from 1 to 5 K. It is  $R_{in} = 7.5$  cm and  $R_{out} = 14.5$  cm. The outer cylinder is made of acrylic glass and accessible for Particle Image Velocimetry (PIV). The inner cylinder is made of anodized aluminum in order to suppress disturbing optical reflection. Both horizontal end-plates are connected to the outer cylinder.

On the upper endplate 12 Peltier elements have been installed. Six of them operate as heat source and were mounted in hexagonal order at the inner part of the plate. All further Peltier elements work as cooling system. They are mounted on top of aluminum blocks. Water is cooled inside the aluminum blocks and continuously pumped downward into a reservoir mounted below the bottom aluminum end-plate to cool the end-plate and keep its temperature constant. The inner and outer cylinders are driven independently by two DC motor units. The vertical temperature profile is analyzed with an infrared camera. Flow velocity measurements are done with a corotating mini-PIV system with a green laser module and a corotating camera. The tank is filled with silicone oil M5 with a Prandtl number of  $Pr = 58$ . This rather high value should allow a comparison with the linear system of equations used below which is valid for very large Prandtl numbers,  $Pr \rightarrow \infty$ . The setup is described in more detail in Seelig et al. (2016).

It is known that strong shear layers develop in TC experiments with endplates. The

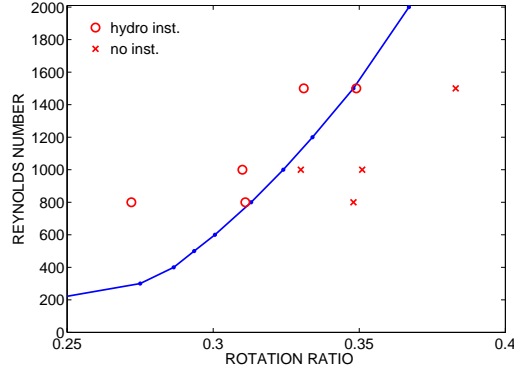


FIGURE 2. Above the numerically simulated solid line the endplate effects of the SRI experiment with  $N = 0$  lead to a nonaxisymmetric instability pattern dominated by the  $m = 2$  mode due to shear layer instability, confirmed by measurements: circles denote instability, crosses stability.

resulting meridional circulation disturbs the flow and modifies the Couette profile close to the endplates. For strong enough differential rotation this shear layers become unstable and nonaxisymmetric modes with  $m > 1$  develop (Avila et al. 2008, Avila 2012). Adding stratification suppresses this instability and reduces the shear layer and the related circulations for quasi-Keplerian flows and steeper profiles (Leclercq et al. 2016). Both effects might appear in the experiment and it is difficult to say how strong the stratification must be in order to stabilize the shear layer. To exclude any interactions between both phenomena, the whole region where shear layers become unstable in unstratified flow is neglected in the further analysis. We therefore probed the stability of the unstratified flow. The results are shown in Fig. 2 in comparison with nonlinear numerical simulations with the code by Gellert & Rüdiger (2009). Unstable flow in the experiment is found above the line that marks the onset of the shear layer instability of the in our geometry most unstable mode  $m = 2$  in simulations.

### 3. The Taylor-Couette flow model

We have to formulate the basic state with prescribed velocity profile  $\mathbf{U} = (0, R\Omega(R), 0)$  and given density vertical stratification  $\rho_0(z)$ . The equations for the background density and azimuthal flow profile take the form

$$\frac{U_\phi^2}{R} = \frac{1}{\rho} \frac{\partial P}{\partial R}, \quad \frac{1}{\rho} \frac{\partial P}{\partial z} = -g, \quad (3.1)$$

and

$$\frac{\partial^2 U_\phi}{\partial R^2} + \frac{1}{R} \frac{\partial U_\phi}{\partial R} - \frac{U_\phi}{R^2} = 0. \quad (3.2)$$

The last equation yields

$$\Omega = a + \frac{b}{R^2}, \quad (3.3)$$

for the angular velocity where  $a$  and  $b$  are free constants. The second term in (3.3) is curl-free hence it has been called as the potential flow. With respect to the theory of the Taylor-Couette flows it defines the Rayleigh limit. The two free constants can be fixed by the boundary values  $\Omega_{\text{in}}$  and  $\Omega_{\text{out}}$  of the angular velocity of the inner cylinder (radius

$R_{\text{in}}$ ) and the outer cylinder (radius  $R_{\text{out}}$ ). It follows

$$a = \Omega_{\text{in}} \frac{\mu - \eta^2}{1 - \eta^2}, \quad b = \Omega_{\text{in}} R_{\text{in}}^2 \frac{1 - \mu}{1 - \eta^2} \quad (3.4)$$

with

$$\mu = \frac{\Omega_{\text{out}}}{\Omega_{\text{in}}}, \quad \eta = \frac{R_{\text{in}}}{R_{\text{out}}}. \quad (3.5)$$

The potential flow at the Rayleigh limit is defined by  $a = 0$ , i.e.  $\mu = \eta^2$ . The above mentioned statement about the role of  $\Omega \propto 1/R$  as the smoothest unstable rotation law might be reformulated (see below).

From (3.1) follows

$$R\Omega^2 \frac{\partial \rho_0}{\partial z} + g \frac{\partial \rho_0}{\partial R} = 0, \quad (3.6)$$

if the rotation law is forced to be independent of  $z$ . From (3.6) one finds  $\partial \rho_0 / \partial R = -\epsilon \partial \rho_0 / \partial z$  with the ratio  $\epsilon = R\Omega^2 / g$  of centrifugal acceleration to the gravity. Only for small  $\epsilon$  in rotating fluids the radius-dependence of  $\rho_0$  can be neglected. This is not possible for accretion disks.

The Froude number as the ratio between the rotation rate  $\Omega_{\text{in}}$  of the inner cylinder and the buoyancy frequency  $N$ ,

$$Fr = \frac{\Omega_{\text{in}}}{N} \quad \text{with} \quad N = \sqrt{-g \frac{\partial \log \rho_0}{\partial z}}, \quad (3.7)$$

represents a normalized rotation rate. The standard Reynolds number is

$$Re = \frac{\Omega_{\text{in}} R_{\text{in}} D}{\nu} \quad (3.8)$$

and stratification Reynolds number with the buoyancy frequency is

$$Rn = \frac{N R_{\text{in}} D}{\nu}, \quad (3.9)$$

hence  $Fr = Re / Rn$ . The gap width is  $D = R_{\text{out}} - R_{\text{in}}$ .

For the normalized centrifugal force  $\epsilon$  one finds

$$\epsilon = Fr^2 R \frac{d \log \rho_0}{dz} \simeq Fr^2 \frac{Rg}{c_{\text{ac}}^2} \quad (3.10)$$

with  $c_{\text{ac}}$  as the speed of sound which for water is more than  $10^5$  cm/s. Hence,  $Rg/c_{\text{ac}}^2$  is  $O(10^{-6})$  for  $R \simeq 10$  cm. The condition  $\epsilon \ll 1$  is thus always fulfilled at least for water.

In cylindric geometry the Boussinesq form of the system of hydrodynamic equations is

$$\begin{aligned} \frac{\partial u_R}{\partial t} + \Omega \frac{\partial u_R}{\partial \phi} - 2\Omega u_\phi &= -\frac{\partial}{\partial R} \left( \frac{p}{\rho_0} \right) + \nu \left( \Delta u_R - \frac{2}{R^2} \frac{\partial u_\phi}{\partial \phi} - \frac{u_R}{R^2} \right), \\ \frac{\partial u_\phi}{\partial t} + \Omega \frac{\partial u_\phi}{\partial \phi} + \frac{1}{R} \frac{\partial R^2 \Omega}{\partial R} u_R &= -\frac{1}{R} \frac{\partial}{\partial \phi} \left( \frac{p}{\rho_0} \right) + \nu \left( \Delta u_\phi + \frac{2}{R^2} \frac{\partial u_R}{\partial \phi} - \frac{u_\phi}{R^2} \right), \\ \frac{\partial u_z}{\partial t} + \Omega \frac{\partial u_z}{\partial \phi} &= -\frac{\partial}{\partial z} \left( \frac{p}{\rho_0} \right) - g \frac{\rho}{\rho_0} + \nu \Delta u_z, \\ \frac{\partial}{\partial t} \left( \frac{\rho}{\rho_0} \right) + \Omega \frac{\partial}{\partial \phi} \left( \frac{\rho}{\rho_0} \right) - \frac{N^2}{g} u_z &= 0 \end{aligned} \quad (3.11)$$

with  $\Delta F = \partial^2 F / \partial R^2 + (1/R) \partial F / \partial R + (1/R^2) \partial^2 F / \partial \phi^2 + \partial^2 F / \partial z^2$  and  $\text{div } \mathbf{u} = 0$  (see

Shalybkov & Rüdiger 2005). Note that there is no molecular diffusion coefficient except viscosity in the system so that the microscopic Schmidt number (equivalent to our Prandtl number) is infinity. Park & Billant (2013) work with  $Sc = 700$ , thus our approximation should be not too far from that.

For homogeneous  $N$  the coefficients of the system only depend on the radial coordinate, so that a normal mode expansion of the solution,  $F = F(R)\exp(i(m\phi + kz - \omega t))$  can be used for all fluctuating quantities. The no-slip boundary conditions at the inner and outer cylinder ( $u_R = u_\phi = u_z = 0$ ) complete the classical eigenvalue problem.

A linear code is used to solve the set of ordinary differential equations for the radial profiles of flow, density and pressure which results in a Fourier mode analysis of the fluctuations. The solutions are optimized with respect to that wave number  $k$  which provides the lowest Reynolds number. The wave numbers are normalized with the characteristic radius  $R_0 = \sqrt{R_{\text{in}}D}$  (which for  $\eta = 0.52$  is very close to the gap width  $D$ ) and the Fourier frequencies with the rotation rate  $\Omega_{\text{in}}$  of the inner cylinder.

#### 4. Potential flow

We start with the discussion of the conditions for neutral instability in the  $(Rn/Re)$  plane of the nonaxisymmetric modes. Neutral instability means vanishing growth rates. The shear numbers  $\mu$  are always considered as free parameters. The most prominent example for the instability is that for potential flow with  $\mu = 0.27$  ( $\mu = \eta^2$ ). Figure 3 shows the combination of the eigenvalues of the solutions of the system of equations (3.11). The potential flow proves to be very unstable against nonaxisymmetric perturbations with low mode numbers  $m$ . The lines of neutral instability are almost-straight lines with  $Fr \simeq \text{const}$ . Obviously, the sufficient and necessary condition for instability of the potential flow against nonaxisymmetric perturbations is

$$Fr_{\min} < Fr < Fr_{\max} \quad (4.1)$$

with  $Fr_{\min} \simeq 0.3$  and  $Fr_{\max} \simeq 5.5$  for  $m = 1$ , i.e. the Froude number  $Fr$  does not even vary over two orders of magnitude. The form of the instability curves suggests the assumption that this condition also holds for very large Reynolds numbers, i.e. in the diffusion-less limit  $\nu \rightarrow 0$ . Le Dizes & Riedinger (2010) argue that the instability of the stratified potential flow is the most unstable one. Our numerical results suggest that all rotation laws with  $\mu \lesssim 0.42$  (the quasi-Keplerian flow with  $\mu = 0.37$  included) belong to this instability class which may also exist without viscosity.

For given  $Rn$  there are always two Reynolds numbers  $Re$  limiting the unstable area. The difference  $\delta Re$  between the maximum and the minimum  $Re$  increases for increasing  $Rn$  but decreases with increasing  $\mu$ .

Figure 3 (left) also shows the instability domains of the modes with  $m = 2$  and  $m = 3$  which are close to the curve for  $m = 1$ . The latter encloses the curve for  $m = 2$  which itself encloses the curve for  $m = 3$ . For the upper branch in the  $(Rn/Re)$  plane representing the solutions for fast rotation the different lines are easy to see while they are much more close together at the lower branch. This finding means that strong shear has a stronger stabilizing effect to the modes with higher  $m$  than for  $m = 1$ . We shall see below that this phenomenon is more effective for flatter rotation laws.

In the right panel of Fig. 3 the wave numbers along the lines of neutral stability are given for the modes  $m = 1, 2, 3$ . The lower parts of the profiles belong to the upper branches of the bifurcation lines and vice versa. Only the models of fast-rotation branch show the well-known Taylor-Proudman theorem so that for faster rotation the cells become elongated in axial direction. The same is not true for the models of the upper,

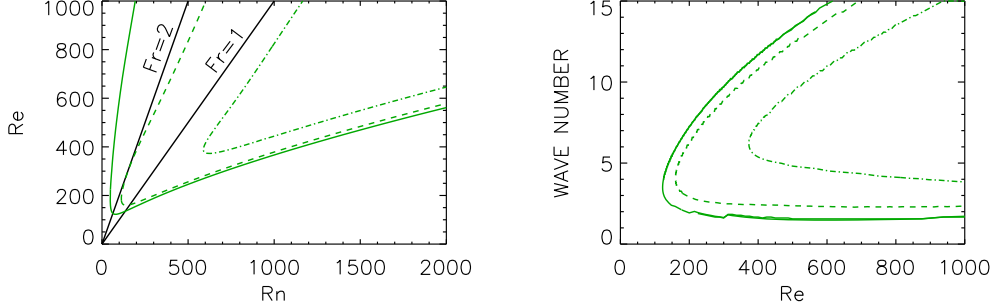


FIGURE 3. Left: Stability map for  $m = 1$  (solid),  $m = 2$  (dashed) and  $m = 3$  (dot-dashed) in the  $(Rn/Re)$  plane for the potential flow ( $\mu = 0.27$ ). The black solid lines display  $Fr = 1$  and  $Fr = 2$ . Right: The wave numbers along the lines of neutral instability. The upper (lower) lines belong to the slow (fast) rotation branches of the map.  $\eta = 0.52$ .

fast-rotation branch along which the wave numbers of all modes are not influenced at all by the rotation. Only for very high Reynolds number the wave numbers slightly increase with  $Re$  producing prolate cell structures.

The azimuthal drift of the nonaxisymmetric instability pattern is considered next. The drift rates are represented by the real part  $\omega_{dr}$  of the frequency  $\omega$  of the Fourier mode normalized with the rotation rate of the inner cylinder. Because of the definition

$$\frac{\dot{\phi}}{\Omega_{in}} = \frac{\omega_{dr}}{m\Omega_{in}} \quad (4.2)$$

the azimuthal migration (4.2) has the same sign of  $\omega_{dr}$ . As the drift rates shown in Fig. 4 (left panel) are always positive the patterns migrate in positive  $\phi$ -direction. Note that the frequencies are normalized with the inner rotation rates. Hence, a drift value of  $\mu$  would describe an exact corotation of the instability pattern with the outer cylinder. After Fig. 4 this condition is almost fulfilled for the solutions. The positive deviation from the value  $\mu$  makes the pattern slightly faster rotating than the outer cylinder.

The drift (4.2) for the potential flow along the lower branch of the instability cone proves to be independent of  $Rn$ . The numerical values show a slight increase towards large  $Rn$ . It is thus suggestive here that  $\lim_{\nu \rightarrow 0} \dot{\phi}/\Omega_{in} = \eta$  for  $\nu \rightarrow 0$  along the lower branch of the instability cone. Let us assume that solutions exist for inviscid fluids, i.e.  $Re \rightarrow \infty$  and  $Rn \rightarrow \infty$ . For the potential flow it is  $\mu = \eta^2$ . There is no other free parameter describing the system than the inner radius  $\eta$ . It is then suggestive that the drift rate is also determined by a function of the inner radius  $\eta$ . The simplest possibility is the linear relation  $\dot{\phi}/\Omega_{in} = \eta$  whose existence is indeed confirmed by the numerical simulations. Figure 4 (right panel) presents the values of (4.2) as functions of  $\mu$  for three models with wide, medium and narrow gaps. The lines demonstrate a linear relation of the azimuthal drift and the shear  $\mu$ . They always start with the potential flow  $\mu = \eta^2$ . Their drift values are indeed close to the dotted line  $\dot{\phi}/\Omega_{in} = \sqrt{\mu}$ . Using  $\mu = \eta^2$  it becomes

$$\frac{\dot{\phi}}{\Omega_{in}} \simeq \eta \quad (4.3)$$

for solutions with large Reynolds numbers. Note that the straight lines stop for too weak differential rotation (marked by diamond).

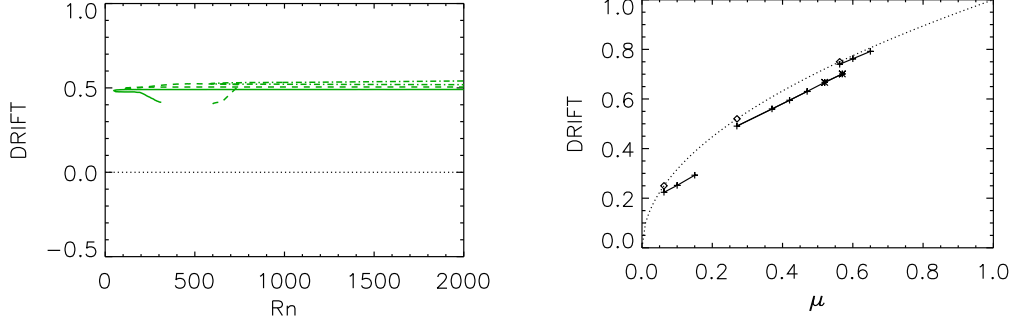


FIGURE 4. Left:  $\omega_{\text{dr}}$  normalized with  $\Omega_{\text{in}}$ .  $\eta = 0.52$ ,  $\mu = 0.27$ ,  $m = 1/2/3$  (solid/dashed/dot-dashed). Right: The azimuthal migration rate (4.2) as function of  $\mu$  for three models with  $\eta = 0.25$ ,  $\eta = 0.52$ ,  $\eta = 0.75$  (from left to right). The dotted curve gives for the potential flow  $\dot{\phi}/\Omega_{\text{in}} = \eta = \sqrt{\mu}$ .

For given  $\eta$  and  $\mu$  taking into account the right panel of Fig. 4 it follows:

$$\frac{\dot{\phi}}{\Omega_{\text{in}}} \simeq \frac{\mu + \eta}{1 + \eta}, \quad (4.4)$$

which for  $\eta = 0.52$  leads to a slope of 0.66 between drift and shear  $\mu$  (see Fig. 5). The migration value (4.4) always exceeds  $\mu$  so that in general *the pattern migrates slightly faster than the outer cylinder rotates*. With respect to the rotation of the outer cylinder, (4.3) leads to

$$\frac{\dot{\phi}}{\Omega_{\text{out}}} \simeq \frac{1}{\mu} \frac{\mu + \eta}{1 + \eta}, \quad (4.5)$$

so that  $\dot{\phi}/\Omega_{\text{out}} \simeq 1/\eta$  for the potential flow. For very thin gaps this yields  $\dot{\phi} \simeq \Omega_{\text{out}}$  hence instability pattern and outer cylinder are corotating in this limit.

Figure 5 shows a basic agreement between the theoretical prediction (4.4) and the empirical results from measurements with the SRI-container described in Section 2. The empirical drift rate linearly runs with the shear parameter  $\mu$ . The more rigid the rotation the closer are the values of pattern drift and rotation rate of the *outer* cylinder. Small differences between the linear theory and the measurements mainly appear for the steepest rotation laws. Indeed, Fig. 4 (left) shows the drift of the potential flow with  $\mu = \eta^2$  being slightly smaller than the approximation (4.4) predicts. The measured drift values are nevertheless in a very good agreement with those derived from the linear theory.

## 5. Flat rotation laws

In their inviscid theory for unbounded flows Le Dizes & Riedinger (2010) find flows with flat rotation laws ( $\mu > 0.4$ ) as stable. Figure 6 shows the instability lines for the rotation laws with  $\mu \geq 0.27$ . The curves are labeled with the parameter  $\mu$  of the differential rotation. For  $\eta = 0.52$  the quasi-Keplerian flow is represented by  $\mu = 0.37$  and the quasi-galactic rotation law  $U_\phi = \text{const}$  by  $\mu = \eta = 0.52$ .

We found all rotation laws for  $\mu \leq \mu_{\text{max}}$  with  $\mu_{\text{max}} = 0.571$  to be unstable for modest Reynolds numbers. Always two Reynolds numbers exist for fixed stratification between them the flow is unstable. Too fast rotation suppresses the instability. This rotational stabilization is much stronger for the flat rotation laws than it is for the steeper profiles



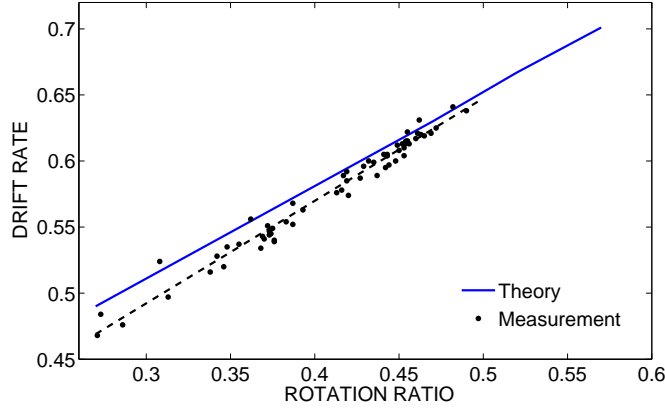


FIGURE 5. Migration rates (4.2) in comparison with the experimental results. The solid blue line gives the linear relation (4.4). The drift always exceeds the rotation ratio  $\mu$  so that the instability pattern overturns the outer cylinder. The slope of the dashed line representing the measurements is 0.77.

close to the  $1/R^2$  law of the potential flow. The transition from strong to weak stabilization lies between  $\mu = 0.42$  and  $\mu = 0.47$  where the curvature of the lines of neutral instability changes. For  $\mu > 0.52$  these lines encircle closed domains which always contain  $Fr = 1$ . The isolines defined by fixed  $\mu$ 's possess two different forms. They are closed if the rotation law is flat and they are open for steep rotation laws. The closed domains with lower Reynolds numbers possess for the same value of  $\mu$  open domains of instability but with much higher Reynolds numbers which seem to be unbounded for  $Re \rightarrow \infty$ . The two domains are separated by a region of stability where the condition  $Fr = 1$  does *not* lead to any linear instability of the mode  $m = 1$ . The phenomenon that certain moderate Reynolds numbers do not lead to an excitation of instability (while for lower  $Re$  and for higher  $Re$  they do) only occurs for the flat rotation laws (Fig. 6).

At  $\mu_{\max} = 0.571$  the lower closed instability domain disappears. For  $\mu > \mu_{\max}$  the SRI can thus only be excited for very large Reynolds numbers, much larger than  $\mathcal{O}(10^3)$ . One finds for example  $Re \simeq 60,000$  for  $\mu = 0.6$ .

Note that  $\mu_{\max} = 0.571$  slightly exceeds  $\mu_{\max} \simeq \eta = 0.52$  suggested by Shalybkov & Rüdiger (2005). Later calculations by Rüdiger & Shalybkov (2009) and also the measurements by Ibanez et al. (2016) showed that the maximum  $\mu$  exceeds the value  $\eta$ , and the present paper limits the excess to  $\simeq 12\%$ .

If the results are represented in the  $(\mu/Re)$  plane used by Ibanez et al. (2016) then the isolines for  $Rn$  have the characteristic form shown in Figs. 7 and 8. Different symbols have here been added representing the empirical results obtained in the SRI experiment described in Section 2. The many rhombs in Fig. 7 (for unstable flows) demonstrate the existence of SRI for a wide range of shear values  $\mu$ , Reynolds numbers  $Re$  and temperature-stratifications  $Rn$ . For given shear and density stratification a lower Reynolds number and an upper Reynolds number exist. All flows with  $Rn < 250$  (black rhombs) should only be unstable in region C which is indeed the case. The blue rhombs for flows with  $250 < Rn < 375$  should not appear in the region A since the rotation there is too fast for the excitation of SRI.

Probably because of endplate effects, the upper  $Re$ -limit is not well-defined. One reason might be that for fast rotation the size of the pattern cells in axial direction would expand beyond the experiment height and the system behaves no longer in accordance with the

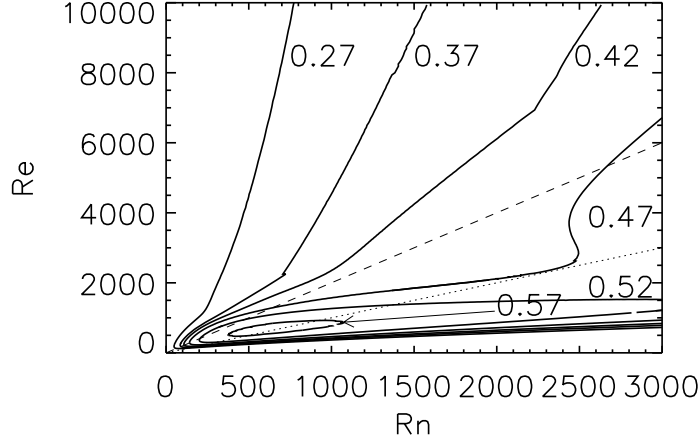


FIGURE 6. Stability maps of the  $m = 1$  mode in the  $(Rn/Re)$  plane. The dotted (dashed) lines mark  $Fr = 1$  ( $Fr = 2$ ). The sign of the curvature of the lines for fast rotation depends on  $\mu$ . The diffusive SRI disappears for  $\mu_{\max} \simeq 0.571$  at  $Re = Rn = 703$ ,  $\eta = 0.52$ .

linear set of equation (see relation (6.3) and its discussion). Note, however, that the measurements precisely confirm the numerically-found slow-rotation limit.

The crosses in Fig. 8 mark experiments without indication of SRI. They define the domains of stability. Because of their definitions no black crosses should appear in region B and no crosses at all should appear in region C. The measurements confirm the expectations.

Rotation laws with SRI excited in the experiments fulfill  $\mu \lesssim 0.49$ . The island solutions for  $\mu \gtrsim 0.50$  with their low growth rates (see Section 8) have not been studied experimentally. The temperature differences of the used SRI experiment do not yet produce the needed high values of  $Rn \simeq 700$ .

The curves of constant  $Rn$  are always crossing each other. Note that there is a turning point in the upper parts of the curves. The curves are concave for steep rotation laws and they are convex for flat rotation laws. Close to the Rayleigh line the rotation only weakly stabilizes the flow. The formal reason is the change of the bending of the neutral lines  $\mu = \text{const}$ , shown in the top corner (left of  $Fr = 2$ ) of Fig. 6 which reflects the transition of open lines for steep rotation laws to closed lines for flat rotation laws. We shall see below that even the wave numbers of these solutions are not reduced by the Taylor-Proudman theorem.

## 6. Cell size and azimuthal drift

The axial size of a cell in units of the gap width  $D$  is

$$\frac{\delta z}{D} \simeq \frac{\pi}{k} \sqrt{\frac{R_{\text{in}}}{D}} \quad (6.1)$$

so that for  $D \simeq R_{\text{in}}$  one finds  $\delta z/D \simeq \pi/k$  with  $k$  as the normalized value of the wave numbers. For large wave numbers the cells are oblate in axial direction. For  $k \simeq \pi$  they will be nearly circular and the short-wave approximation fails. Figure 9 (left) gives the wave numbers along the lines of marginal stability. One finds that the wave numbers

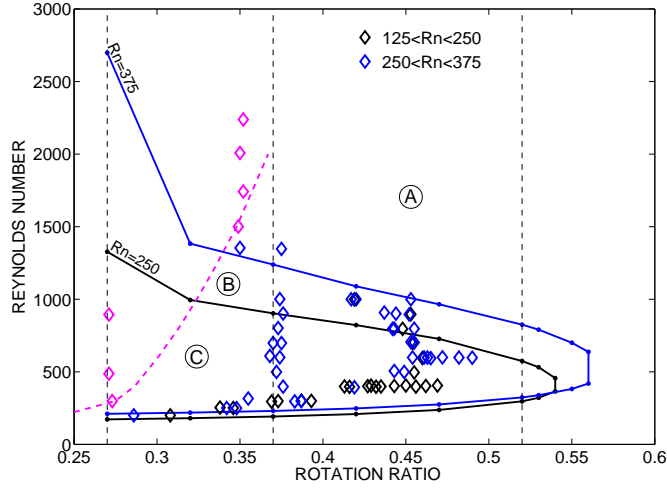


FIGURE 7. Lines of neutral stability for the  $m = 1$  mode in the  $(\mu/Re)$  plane for  $Rn = 250$  (black) and  $Rn = 375$  (blue). The vertical lines stand for  $\mu = 0.27$  (potential flow), for  $\mu = 0.37$  (quasi-Keplerian flow) and  $\mu = 0.52$  (uniform linear flow speed). The empirical results of the SRI experiment described in Section 2 are added with rhombs for observed instability. The pink line corresponds to the domain of strong endplate effects described in Fig. 2, also the measurements in this domain are given by pink symbols.

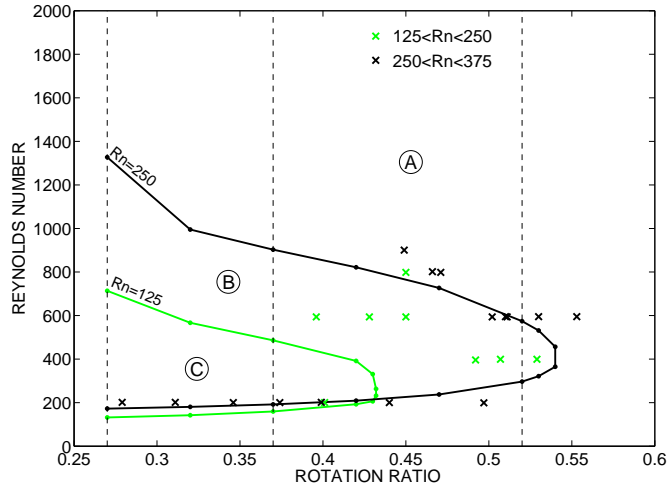


FIGURE 8. Same as in Fig. 7 but for the experiments leading to stable flows (crosses). Green line: neutral stability for  $Rn = 125$ , black line: neutral stability for  $Rn = 250$ .

depend on the Froude number  $Fr$  rather than on the shear value  $\mu$ . The normalized wave number is inversely proportional to the Froude number, i.e.  $k \cdot Fr \simeq 4$ , which with (6.1) yields

$$\frac{\delta z}{D} \simeq \frac{\pi}{4} \frac{\Omega_{in}}{N} \quad (6.2)$$

(see Molemaker et al. 2001). Due to the Taylor-Proudman theorem along the fast-rotation part of the instability map (with  $Fr > 1$ ) the vertical cell sizes are large, questioning the short-wave approximations. The wavelengths for slow rotation and large stratification ( $Fr < 1$ ) are very short.

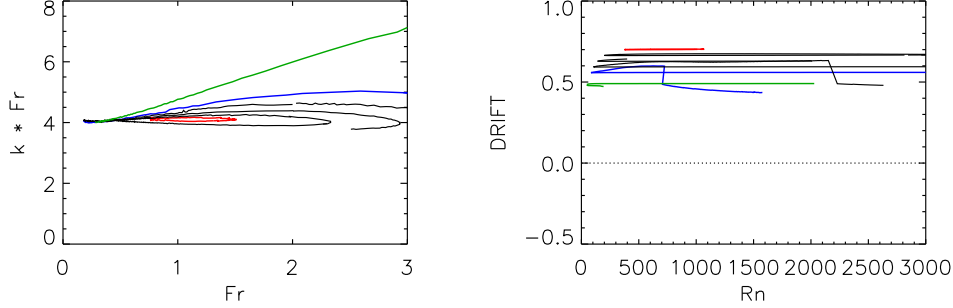


FIGURE 9. Left: Normalized wave numbers  $k \cdot Fr$  along the lines of marginal stability for  $\mu$  between 0.27 and 0.57 as a function of the Froude number  $Fr$ . Right: Drift rates in units of the rotation rate of the inner cylinder. Potential flow (fast-rotating branch, green line), quasi-Keplerian flow (blue line),  $\mu = 0.57$  (red line).  $\eta = 0.52$ .

In the experiments of Ibanez et al. (2016) the relation (6.2) has been probed with the result  $\delta z/D \simeq 0.86 \cdot Fr$  close to our result  $\delta z/D \simeq 0.78 \cdot Fr$ . One can also read the latter relation as

$$Fr = 1.28 \Gamma \frac{\delta z}{H} \quad (6.3)$$

which relates the aspect ratio  $\Gamma$  of a finite-height container to a maximally reasonable  $Fr$ . Provided the minimal number of cells in the container is (only) two then for  $\Gamma = 10$ , the fastest rotation which is reasonable for experiments follows from  $Fr \simeq 6.3$ . With four cells required,  $Fr \simeq 3.1$  would be the upper limit. For the fast-rotation branch of potential flow, however, no such limit exists. The green line in Fig. 9 leads to the fixed wave number  $k \simeq 2.5$  for all  $Fr$  which hardly depends on the rotation rate (see Fig. 3, right panel). In axially bounded containers it makes thus sense to realize the SRI for fast rotation mainly close to the Rayleigh limit. For the potential flow the relation (6.1) reads  $\delta z/D \simeq 1.3$  leading to  $\delta z/H \simeq 1.3/\Gamma$  which for  $\Gamma = 10$  is certainly small enough even for experiments with fast rotation.

Again the drift rates of the patterns of marginal stability do not depend on the location in the  $(Rn/Re)$  plane. The weak dependence on the rotation law in Fig. 9 (right panel) approaches the linear run with  $\mu$  in accordance to (4.4). The simplicity of the results in Fig. 9 is amazing. Along the lines of marginal stability the drift values (4.2) do not vary and the wave numbers are strictly anti-correlated to  $Fr$  with one and the same numerical factor.

## 7. The higher Fourier modes

For quasi-Keplerian rotation the instability domains of the modes with  $m = 1$ ,  $m = 2$  and  $m = 3$  are compared in Fig. 10 (left). The curve for  $m = 1$  encloses the curve for  $m = 2$  which itself encloses the curve for  $m = 3$ . There are no crossing points. For given stratifications and increasing Reynolds numbers the rotation successive stabilizes the higher azimuthal mode numbers. If the rotation is too fast then also the  $m = 1$  mode is no longer unstable. On the other hand, the lower (slow-rotation) branches for various  $m$  are rather close together. Only for fast rotation, therefore, the SRI is a nonaxisymmetric instability of low  $m$ .

The axial wave numbers vary only slightly for various  $m$  if plotted as a function of

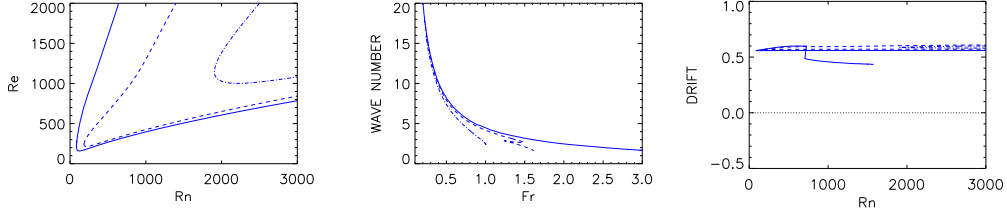


FIGURE 10. Stability map (left), normalized wave numbers (middle) and drift rates (right) for the quasi-Keplerian rotation law for the modes  $m = 1$  (solid),  $m = 2$  (dashed) and  $m = 3$  (dot-dashed). Wave number and Froude number are anti-correlated. The drift values do not depend on the stratification.  $\mu = 0.37$ ,  $\eta = 0.52$ .

$Fr$  (Fig. 10, middle panel). For fast rotation the wave numbers are small while for slow rotation the axial wave numbers are large and the cells are flat. There is only a rather weak dependence of the wave number on the mode number  $m$ . For all  $m$  the wave numbers and the Froude number are anti-correlated. The drift values (4.2) do also not vary too much for  $m = 1, 2, 3$  (Fig. 10, right). The pattern migration of the higher modes does thus not differ from the migration of the  $m = 1$  mode. Hence, the whole patterns always rotate slightly faster than the outer cylinder.

The curves in the right panels of Figs. 9 (where  $\mu$  varies) and 10 (where  $m$  varies) are nearly identical. For all the considered  $\mu$  and  $m$  the azimuthal drift does hardly vary. The same is true for the wave numbers if considered as a function of  $Fr$ . The uniform drift values and the anti-correlation between the wave numbers and the Froude number appear to be the basic characteristics for the modes with low  $m > 0$  as the solution of the equation system (3.11).

## 8. Growth rates

The growth rate is the imaginary part of the eigenfrequency (here normalized with  $\Omega_{in}$ ) and the growth time  $\tau_{gr}$  in units of the rotation time is  $\tau_{gr}/\tau_{rot} = \Omega_{in}/(2\pi\omega_{gr})$ . To find the characteristic growth rates of the instability the wave numbers and frequencies are computed for a given Reynolds number with supercritical  $Rn$ . The Reynolds number is fixed to  $Re = 2000$  for  $\mu = 0.37$  (Fig. 11, left). One finds small values of order 0.01, i.e. the growth time is typically 6 turnovers of the *outer* cylinder. Note that the maximal growth rates exist for  $Fr \lesssim 1$ . The result does not strongly depend on the azimuthal Fourier mode number  $m$ . However, the higher the  $m$  the smaller the interval of  $Rn$  for instability. It is also possible that for certain  $Rn$  the growth rate of a higher mode exceeds that for a lower mode (Fig. 11 at  $Rn \simeq 5000$ ).

The behavior of the drift rates along the line  $Re = 2000$  is also characteristic. The drift rates (4.2) do also not depend on  $m$  nor the value of  $Rn$ . Cell sizes and drift rates are basically equal for the modes with various azimuthal mode numbers (Fig. 11, right).

Close to  $Fr = 1$  the growth rates reach a maximum. One also wants to know whether the growth rates for separated domains of instability for one and the same value of  $\mu$  are similar or not. Another question is the behavior of the growth rate in the limit  $\nu \rightarrow 0$ . In this limit ( $Re \rightarrow \infty$ ) the diffusion time  $\tau_{diff} \simeq D^2/\nu$  becomes infinitely large so that any instability with  $\tau_{gr} \propto \tau_{diff}$  cannot be excited for  $\nu \rightarrow 0$  in finite times. If, however, the growth rate remains finite for  $Re \rightarrow \infty$  then the instability also exists in the inviscid limit, and it is called a fast instability.

Figure 12 gives the results for a rotation law with  $\mu = 0.5$  for nearly uniform azimuthal

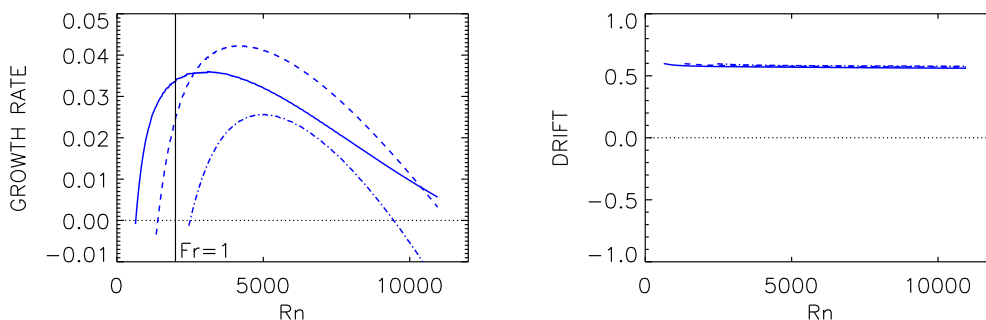


FIGURE 11. Growth rate in units of  $\Omega_{in}$  (left) and drift rate (4.2) (right) for fixed Reynolds number  $Re = 2000$ .  $m = 1$  (solid),  $m = 2$  (dashed),  $m = 3$  (dot-dashed). The vertical line marks  $Fr = 1$ .  $\mu = 0.37$ .

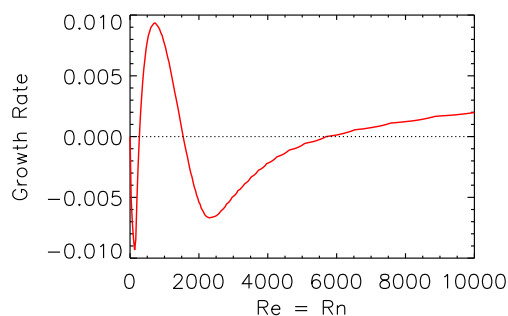


FIGURE 12. Growth rates in units of  $\Omega_{in}$  for  $m = 1$  and  $\mu = 0.5$  along the line  $Fr = 1$ .

velocity  $U_\phi$ . We find that the growth rates in the closed domain exceed the growth rate in the open domain by almost one order of magnitude but they are much smaller than the growth rates in Fig. 11 for more steep rotation laws. SRI for steep rotation laws is thus more easy to find than for flat rotation laws. Additionally, the growth rates seem to remain finite for very large Reynolds numbers. The stratorotational instability is thus a fast instability which should also exist for inviscid fluids.

## 9. Conclusions

In view of the laboratory experiment described in Section 2 the hydrodynamic equation system (3.11) has been solved numerically for the Taylor-Couette flow with the inner cylinder at  $\eta = 0.52$  for various rotation laws. The potential flow gives the simplest example with which the stratorotational instability can experimentally be realized. The critical Reynolds number for onset of SRI for the potential flow with  $\mu = 0.27$  is only 135 and for quasi-Keplerian flow with  $\mu = 0.37$  it is  $Re = 168$ . This trend, however, does not continue to more flat rotation laws. There is a well-defined maximal value of  $\mu = \mu_{max}$  at which the low- $Re$  regime suddenly stops. For larger  $\mu$  the critical Reynolds numbers are higher by orders of magnitudes. The maximum  $\mu_{max}$  increases for narrower gaps. For  $\eta = 0.52$  the value of  $\mu_{max} = 0.571$  indicates that the characteristic rotation

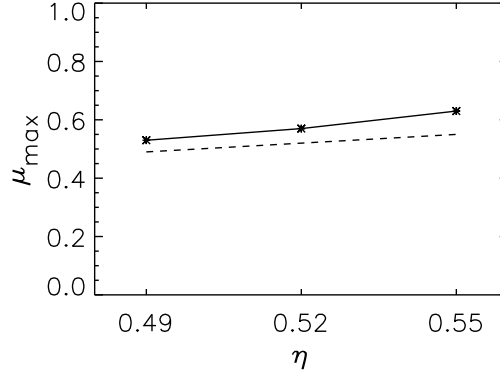


FIGURE 13. The maximal values of  $\mu$  with  $Re < 2000$  for various gap widths  $\eta$ . The dashed line denotes the rotation law with  $\mu = \eta$ . The calculated  $\mu_{\max}$  thus represent rotation laws slightly flatter than  $U_\phi = \text{const.}$

law is slightly flatter than the rotation law with  $\Omega \propto R$ . This finding remains true if the gap width is varied (Fig. 13).

Figure 6 presents the instability map for the shear values of the applied rotation laws. It typically shows a more massive rotational stabilization effect for weak density stratification than for strong density stratification. The effect increases for increasing  $\mu$ , i.e. for flatter rotation laws. The instability map shows two separated domains where the one with the small  $Rn$  is closed and possesses small Reynolds numbers with  $Re = \mathcal{O}(10^3)$ . The second instability area in the map is open for  $Rn \rightarrow \infty$  and moves towards increasing Reynolds numbers for more and more flat rotation laws. For  $\mu > \mu_{\max}$  this instability type requires Reynolds numbers exceeding  $Re = \mathcal{O}(10^5)$ .

Figures 7 and 8 for three different stratification numbers  $Rn$  show the theoretical instability domains for all  $\mu < \mu_{\max}$ . There is always a lower  $Re$  and an upper  $Re$  limiting the instability area. The dependence of the lower limiting  $Re$  on the stratification number  $Rn$  is very weak while it is much stronger for the upper limits. The experimental data added to the plots match these intervals with only a few exceptions at the fast-rotation branches. The low-rotation limit is almost perfectly confirmed by the measurements. The definition of the upper limit for fast rotation is less precise. There are, in particular, unstable flows with Kepler-like rotation laws for Reynolds numbers which should already lead to stability based on the numerical simulations. The wave numbers, however, at the upper line of neutral stability are so small that endplate effects by the apparatus (with aspect ratio  $\Gamma = 10$ ) must be expected. Note that in Fig. 8 all crosses correctly indicate the expected stability for the flatter rotation laws.

Both wave numbers and azimuthal drift of the nonaxisymmetric modes fulfill simple rules. The patterns always drift in the positive  $\phi$ -direction – slightly faster than the outer cylinder rotates. For very narrow gaps ( $\eta \rightarrow 1$ ) the instability pattern would corotate with the outer cylinder. The pattern speed does neither depend on the Reynolds numbers nor on the azimuthal mode number  $m$ . The drift data from the Cottbus SRI experiment indeed demonstrate the rotation of the instability pattern as slightly faster than the rotation of the outer cylinder. The predicted linear relation between drift  $\dot{\phi}$  and rotation ratio  $\mu$  is also confirmed by the experiments. The theory describes the observed migration phenomena of the nonaxisymmetric perturbation flows with high accuracy (see Fig. 5).

One also finds a general rule for the wave numbers. Figure 9 provides the wave numbers

for the modes with  $m = 1$  in the regions of instability as basically behaving as  $k \propto 1/Fr$ . The cells are thus nearly circular in the  $(R/z)$  plane for  $Fr \simeq 1$ . They are prolate for fast rotation with  $Fr > 1$  and they are oblate for slow rotation with  $Fr < 1$ . As an exception, the cells for the potential flow instability are always nearly circular in the  $R/z$  plane independent of the actual Froude number.

M.G. would like to acknowledge support from the Helmholtz alliance *LIMTECH*. T.S., C.E. and U.H. thank DFG for financial support under grant 'Angular momentum transport in a stratified Taylor-Couette experiment with applications to accretion disks' (EG100/18-1, HA 2932/7-1). T.S. and U.H. acknowledge helpful discussions with P. Le Gal. They further thank L. Stapelfeld, V. Ruoff, R. Stöbel and M. Burchardt for support in running and maintaining the experiment and A. Krebs for help regarding calibration and data analysis.

#### REFERENCES

- ARLT, R., & URPIN, V. 2004 Simulations of vertical shear instability in accretion discs. *Astron. Astrophys.* **426**, 755–765.
- AVILA, M., GRIMES, M., LOPEZ, J. M. & MARQUES, F. 2008 Global endwall effects on centrifugally stable flows. *Phys. Fluids* **20**, 104104.
- AVILA, M. 2012 Stability and angular-momentum transport of fluid flows between corotating cylinders. *Phys. Rev. Lett.* **108**, 124501.
- CHAGELISHVILI, G. D., ZAHN, J.-P., TEVZADZE, A. G., & LOMINADZE, J. G. 2003 On hydrodynamic shear turbulence in Keplerian disks: Via transient growth to bypass transition. *Astron. Astrophys.* **402**, 401–407.
- DUBRULLE, B., MARIÉ, L., NORMAND, CH., RICHARD, D., HERSANT, F., & ZAHN, J. P. 2005 A hydrodynamic shear instability in stratified disks. *Astron. Astrophys.* **429**, 1–13.
- GELLERT, M., & RÜDIGER, G. 2009 Stratorotational instability in Taylor-Couette flow heated from above. *J. Fluid Mech.* **623**, 375–386.
- IBANEZ, R., SWINNEY, H.L., & RODENBORN, B. 2016 Observations of the stratorotational instability in rotating concentric cylinders. *preprint*.
- LE BARS, M., & LE GAL, P. 2006 Experimental Analysis of the Stratorotational Instability in a Cylindrical Couette Flow. *Phys. Rev. Lett.* **99**, id. 064502.
- LECLERCQ, C., PARTRIDGE, J.L., AUGIER, P., DALZIEL, S.B., & KERSWELL, R.R. 2016 Using stratification to mitigate end effects in quasi-Keplerian Taylor-Couette flow. *J. Fluid Mech.* **791**, 608–630.
- LE DIZES, S., & RIEDINGER, X. 2010 The stratorotational instability of Taylor-Couette and Keplerian flows *J. Fluid Mech.* **660**, 147–161.
- MOLEMAKER, M. J., MCWILLIAMS, J. C., & YAVNEH, I. 2001 Instability and Equilibration of Centrifugally Stable Stratified Taylor-Couette Flow. *Phys. Rev. Lett.* **86**, 5270–5273.
- PARK, J., & BILLANT, P. 2013 The stably stratified Taylor-Couette flow is always unstable except for solid-body rotation. *J. Fluid Mech.* **725**, 262–280.
- RÜDIGER, G., & SHALYBKOV, D. 2009 Stratorotational instability in MHD Taylor-Couette flows. *Astron. Astrophys.* **493**, 375–383.
- SEELIG, T., BURCHARDT, M., KREBS, A., HARLANDER, U. & EGBERS, CH. 2016 PIV measurements in an axially stratified Taylor-Couette experiment. In: *Lasermethoden in der Strömungsmesstechnik - 24. Fachtagung der GALA e.V. 2016, GALA e.V., BTU Cottbus – Senftenberg*, 13.1–13.8., ISBN 978-3-9816764-2-6
- SHALYBKOV, D., & RÜDIGER, G. 2005 Stability of density-stratified viscous Taylor-Couette flows. *Astron. Astrophys.* **438**, 411–417.
- TEVADSE, A.G., CHAGELISHVILI, G.D., & ZAHN, J.-P. 2008 Hydrodynamic stability and mode coupling in Keplerian flows. *Astron. Astrophys.* **478**, 9–15.
- UMURHAN, O. M. 2006 On the stratorotational instability in the quasi-hydrostatic semi-geostrophic limit. *Mon. Not. R. Astron. Soc.* **365**, 85–100.



- URPIN, V., & BRANDENBURG, A. 1998 Magnetic and vertical shear instabilities in accretion discs . *MNRAS* **294**, 399–406.
- WITHJACK, E. M., & CHEN, C. F. 1974 An experimental study of Couette instability of stratified fluids. *J. Fluid Mech.* **66**, 725–737.
- YAVNEH, I., MCWILLIAMS, J. C., & MOLEMAKER, M. J. 2001 Non-axisymmetric instability of centrifugally stable stratified Taylor-Couette flow. *J. Fluid Mech.* **448**, 1–21.